Nanoscale

PAPER

View Article Online
View Journal | View Issue

Cite this: *Nanoscale*, 2015, **7**, 11075

Aqueous synthesis of PEGylated copper sulfide nanoparticles for photoacoustic imaging of tumors†

Ke Ding,[a,c] Jianfeng Zeng,[b,c] Lihong Jing,[a] Ruirui Qiao,*[a,c] Chunyan Liu,[a] Mingxia Jiao,[a] Zhen Li[b,c] and Mingyuan Gao*[a,c]

Received 5th April 2015,
Accepted 13th May 2015

DOI: 10.1039/c5nr02180d

www.rsc.org/nanoscale

By integrating high imaging sensitivity and high resolution in a single modality, photoacoustic (PA) imaging emerges as a promising diagnostic tool for clinical applications. Benefiting from the absorption in the near-infrared region (NIR), copper sulfide nanoparticles (NPs) as a contrast agent are potentially useful for increasing the sensitivity of PA imaging. However, the aqueous synthesis of size-tunable, biocompatible and colloidally stable copper sulfide NPs remains challenging due to the intrinsic dipole–dipole interactions among particles. In this work, aqueous synthesis of PEGylated copper sulfide NPs with controllable size between 3 and 7 nm was developed. The particle size-dependent contrast enhancement effect of the copper sulfide NPs for PA imaging was carefully studied both *in vitro* and *in vivo*. Although the contrast enhancement effect of the copper sulfide NPs is proportional to particle size, the *in vivo* studies revealed that copper sulfide NPs smaller than 5 nm presented higher tumor imaging performance, especially at the tumor boundary site, which was further discussed in combination with the pharmacokinetic behaviors of differently sized particles.

Introduction

Photoacoustic (PA) imaging is a newly emerging biomedical modality that provides both high spatial resolution and strong biochemical contrast, benefiting from the combined merits from ultrasound imaging and optical imaging.[1–4] Based on the ultrasonic signal generated from the PA effect, it is possible to obtain high spatial resolution images with optical contrast in a region up to 5–6 cm deep in biological tissues, which breaks through the optical diffusion limit.[5,6] Meanwhile, PA imaging provides inherently background-free detection attributed to the fact that nonabsorbing tissue components present no background, and it overcomes the speckle artifact of ultrasound imaging.[3,7] Relying on the endogenous optical absorbers in different tissues, especially the rich optical absorption from oxyhemoglobin and deoxyhemoglobin in red blood cell, numerous applications by using PA imaging have been exploited for visualizing biological structures at an anatomical or even functional level.[8–10]

To further enhance the contrast in PA images, exogenous absorbers in the NIR region known as PA contrast agents are intensely investigated over the past decade.[1] Owing to the intrinsic absorptive properties, plasmonic nanomaterials, such as gold nanocrystals are widely applied as potential PA contrast agents.[5,11–13] However, relatively large sizes (>35 nm TEM size) are commonly needed to obtain absorption in the NIR region for the above-mentioned nano-absorbers, resulting in rapid clearance by the reticuloendothelial (RES) system from intravenous delivery.[5] Thus, the imaging performance is largely limited by the poor bioavailability of the contrast agents (herein, the bioavailability means an effective accumulation of the nanoparticles delivered through intravenous injection at the tumor site for imaging). Benefiting from the strong localized surface plasmon resonance (LSPR) effect originating from free holes, copper sulfide nanoparticles provide an alternative to Au particle-based photoacoustic contrast agent due to its inherent low hole density and high hole effective mass.[14–17] In addition, its size-dependent NIR absorption behavior in the small size regime (<10 nm) favors the *in vivo* bioapplications for tumor imaging.[15,18–21]

Apart from the significant PA contrast enhancement effect of small copper sulfide NPs, water solubility and colloidal

[a]*Institute of Chemistry, Chinese Academy of Sciences, Bei Yi Jie 2, Zhong Guan Cun, Beijing 100190, China. E-mail: gaomy@iccas.ac.cn, qiaorr@iccas.ac.cn*
[b]*School of Radiation Medicine and Protection, Medical College of Soochow University, 199 Ren-Ai Road, Suzhou Industrial Park, Suzhou 215123, China*
[c]*Collaborative Innovation Center of Radiation Medicine of Jiangsu Higher Education Institutions, 199 Ren-Ai Road, Suzhou Industrial Park, Suzhou 215123, China*

† Electronic supplementary information (ESI) available: XRD results, theoretical hydrodynamic size, temporal evolution of TGA-capped copper sulfide NPs, concentration-dependent growth-inhibition of HeLa cells. See DOI: 10.1039/c5nr02180d

stability are basic requirements for their applications in a biological system. Up to now, the synthesis of water-soluble copper sulfide NPs is mainly achieved through two synthetic routes: indirect organic-phase synthesis followed by a ligand-exchange process, and direct aqueous-phase synthesis. Albeit yielding high-quality NPs with narrow size distribution and high crystallinity, the organic-phase synthetic route is strongly limited by the high-cost, unfriendly experimental conditions and complicated ligand-exchange process.[22–26] Alternatively, the direct aqueous synthetic route provides a greener approach for acquiring water-soluble copper sulfide NPs.[27–29] Nevertheless, due to the inherent dipole–dipole interaction, strong interactions among the NPs often lead to particle aggregation.[25,30,31] Consequently, it remains challenging to develop an efficient synthetic strategy for achieving aqueous copper sulfide NPs with excellent colloidal stability and size tunability.

Following on from our previous studies on the synthesis of copper chalcogenide and their *in vivo* tumor imaging applications,[31–33] herein we report our recent results on the aqueous synthesis of water-soluble copper sulfide NPs with controllable size between 3 and 7 nm. The thoil-poly(ethylene glycol) (HS-PEG) was introduced as a surface ligand for providing water solubility, colloidal stability as well as biocompatibility. The effects of particle size on the optical properties, cytotoxicity and *in vivo* PA imaging of tumor were investigated.

Experimental section

Chemicals

Copper(I) chloride (CuCl, 97%), thioacetamide (TAA, 99%), and sodium hydroxide (NaOH, 96%) were purchased from Alfa Aesar. Thiol-PEG (HS-PEG, molecular weight 2000) was purchased from Tianjin Goldenbio Co., Ltd. Ether and ethanol were of analytical reagent grade and purchased from Sinopharm Chemical Reagent Beijing Co., Ltd. Millipore quality deionized water (Milli-Q water) (resistivity is 18.2 MΩ cm) was utilized in the experiments. 3-(4,5-Dimethylthiazol-2-yl)-2,5-diphenyl tetrazolium bromide (MTT, 98%), dimethyl sulfoxide (DMSO), Dulbecco's modified Eagle medium (DMEM, high glucose), and fetal bovine serum (FBS) were bought from Biodee Biotechnology Co., Ltd, Beijing, China. Other solvents and chemicals were used without further purification.

Synthesis of the PEGylated copper sulfide NPs

In brief, 0.6 g (0.3 mmol) of HS-PEG was dissolved in 15 mL of water, and then 0.015 g (0.15 mmol) of CuCl was introduced while stirring. Nitrogen gas was introduced to purge the reaction solution for 1 h. The pH value of the reaction mixture was adjusted to 9.00 by dropwise addition of 0.5 M NaOH aqueous solution. After that, 0.0056 g (0.075 mmol) of TAA was then introduced while stirring. The resulting mixture was then heated to 90 °C, and the reaction was allowed for 17 h under nitrogen protection. During this process, the color of the reaction solution progressively changed from light yellow to yellow, orange, and finally dark brown. A series of aliquots were extracted at 90 °C for monitoring the particle growth. Then the solution was cooled to room temperature. Upon addition of ethanol into the resulting solution (vol : vol = 2 : 1), the resulting NPs were precipitated in ether and isolated by centrifugation. By being redispersed in ethanol and subsequently precipitated with ether for three cycles, the nanocrystals finally obtained were redispersed in water for further experiments. The particle solution was subsequently purified by ultrafiltration at 5000*g* using a 10 kDa ultrafiltration device (Millipore). The condensed solution was then ready for further experiments.

Cytotoxicity assay of the PEGylated copper sulfide NPs

MTT assays were performed to assess the cytotoxicity of the copper sulfide NPs. Specifically, HeLa cells were first seeded in 96-well plates at a density of 4000 cells per well and cultured for about 24 h in DMEM supplemented with 10% FBS. Then, the cells were washed with PBS and incubated with copper sulfide NPs at different concentrations at 37 °C for 24 h. Subsequently, the cells were washed twice with PBS followed by further proliferating in the culture medium for 48 h; subsequently, 20 μL of MTT with a concentration of 5 mg mL^{-1} was added and allowed to react with the cells for 4 h before the addition of 150 μL of DMSO for dissolving the precipitation. Finally, the absorption of each solution was measured at 490 nm on a microplate reader (Thermo, Varioskan Flash).

Animal model

The tumor models used were established upon subcutaneous injection of HeLa cells ($\sim 5 \times 10^6$) into male BALB/c nude mice (4–6 weeks old) at the flank region of the right hind leg. The tumor imaging studies were carried out 10 days after the inoculations of tumor cells.

All animal experiments reported herein were carried out according to a protocol approved by the Peking University Institutional Animal Care and Use Committee.

Photoacoustic (PA) imaging

In vitro PA images of PEGylated copper sulfide NPs in different concentrations were acquired using a multispectral optoacoustic tomography system (iThera Medical, inVision 256) at a wavelength of 850 nm. For *in vivo* PA imaging studies, a nude mouse bearing subcutaneous tumors was anesthetized by 1% isoflurane delivered *via* a nose cone, and then the PEGylated copper sulfide NPs (3 mg Cu per kg body weight) were injected *via* the tail vein. *In vivo* PA images were acquired at different time points post injection using the multispectral optoacoustic tomography system at a wavelength of 850 nm. The averaged PA signals of tumor regions were extracted using the multispectral optoacoustic tomography software.

Pharmacokinetics of the PEGylated copper sulfide NPs

Male, 6-week-old Sprague Dawley rats were adopted for the pharmacokinetic studies of differently sized PEGylated copper sulfide NPs after they were intravenously injected into groups

of rats (n = 4). The dose level was the same as that for imaging experiments. Blood samples were obtained *via* retro-orbital blood collection at 5 min, 15 min, 30 min, 1 h, 2 h, 4 h, 6 h, 8 h, 24 h, and 48 h post-injection. The red blood cells were removed from the collected blood by centrifugation at 1000 rpm. The blood was weighed, and eroded with concentrated nitric acid and H_2O_2 for measuring the Cu content in the plasma with ICP-OES.

Characterization

Absorption spectra were recorded at room temperature on a Cary 50 UV-Vis spectrophotometer. Transmission electron microscopy (TEM) images were taken on FEI Tecnai20 and JEM-2100F microscopes working at an accelerating voltage of 200 kV. The metal composition was determined by the Inductively Coupled Plasma Optical Emission Spectrometer (ICP-OES) method using a Thermo Fisher IRIS Intrepid II XSP. Powder X-ray diffraction (XRD) patterns were obtained with a Regaku D/Max-2500 diffractometer equipped with Cu Kα1 radiation (λ = 1.54056 Å). Dynamic light scattering (DLS) measurements were carried out at 298.0 K with a Nano ZS (Malvern) equipped with a solid-state He–Ne laser (λ = 633 nm) for measuring the hydrodynamic size of the resulting NPs. PA imaging was performed using a multispectral optoacoustic tomography system (iThera Medical, inVision 256).

Results and discussion

Synthesis and characterization of the PEGylated copper sulfide NPs

In brief, the PEGylated copper sulfide NPs were prepared by heating the reaction mixture of CuCl and TAA at 90 °C in the presence of HS-PEG in water of pH = 9.00. HS-PEG was serving as a capping agent to ensure the water solubility of the NPs. Through a slow hydrolysis of TAA, differently sized NPs were obtained by different reaction times. Fig. 1 presents the TEM images of the resulting NPs obtained at the reaction times of 1 h, 5 h, and 17 h. The NPs are uniform with average particle sizes of 2.7 nm, 4.8 nm, and 7.2 nm, respectively. The resulting NPs presented a crystalline structure close to chalcocite by XRD as displayed in Fig. S1 in the ESI.† Owing to the long chain of HS-PEG ligands,[34] the overall size of the NPs from the current reaction is much smaller than those prepared by using small molecular surface capping agents such as sodium citrate.[18] Further particle size analysis reveals that the relative standard deviation firstly decreased for particles and then slightly increased, *i.e.* 14.8% (2.7 nm), 10.4% (4.8 nm) and 11.1% (7.2 nm). With further prolonged reaction time, the particle size distribution greatly increased, which suggests that the Ostwald ripening process started to play a determining role governing the particle size.[35] Therefore, the above particle samples, denoted as CS-2.7, CS-4.8 and CS-7.2, were chosen for the following studies on particle size-dependent optical properties, cytotoxicity and tumor imaging performance together with pharmacokinetic behaviors.

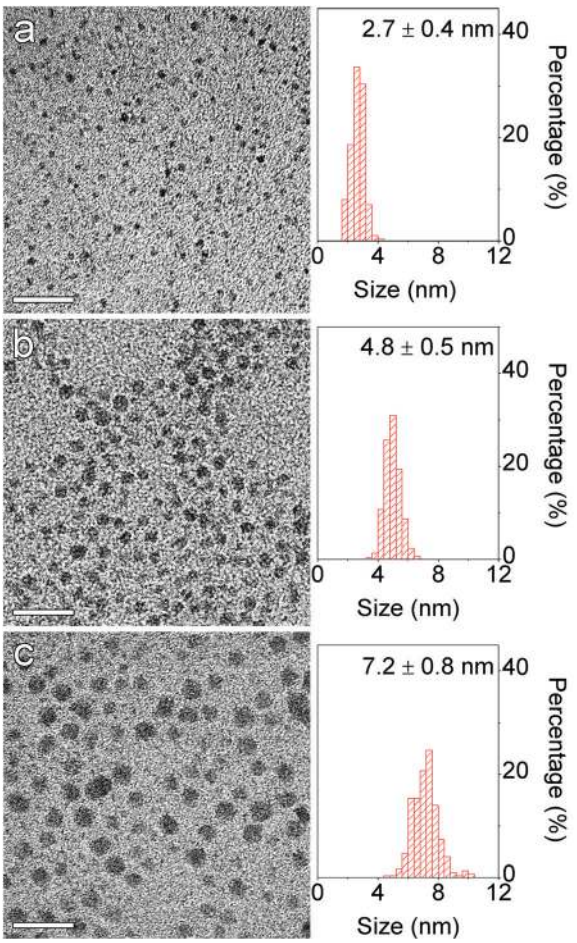

Fig. 1 TEM images of PEGylated copper sulfide NPs acquired at reaction times of 1 h (a), 5 h (b), and 17 h (c), respectively, together with the corresponding size histograms. All scale bars correspond to 20 nm.

Optical properties of the PEGylated copper sulfide NPs

For PA imaging application, the contrast enhancement performance of copper sulfide NPs strongly depends on their optical properties.[14,36] As displayed in Fig. 2, copper sulfide NPs present a broad NIR absorption band that can be attributed to the LSPR effect arising from free holes originating from the copper vacancy.[14,16] Theoretically, the LSPR energy is proportional to the copper vacancy density,[14] which explains the strong particle size-dependent LSPR intensity shown in Fig. 2 as well as the strongest LSPR intensity of CS-7.2.

Colloidal stability of the PEGylated copper sulfide NPs

To evaluate the colloidal stability of the as-prepared NPs, the hydrodynamic sizes of PEGylated copper sulfide NPs dispersed in water and PBS buffer were characterized by DLS. As shown in Fig. 3a, all particle samples exhibit single scattering peaks in water located at 7.1 nm, 10.7 nm, and 14.9 nm for CS-2.7, CS-4.8, and CS-7.2, respectively. Moreover, the experimental hydrodynamic sizes are in good agreement with the theoretical predictions as listed in Table S1,† indicating that the PEGy-

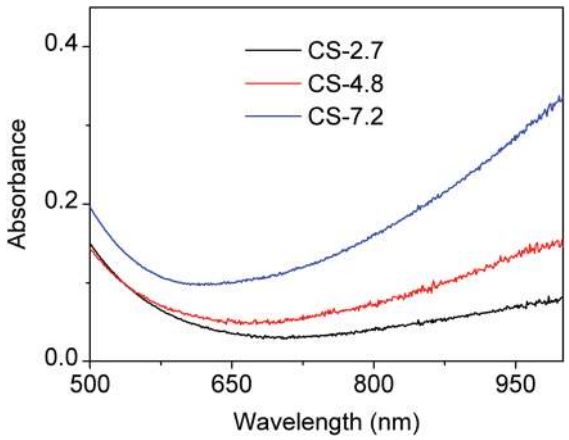

Fig. 2 Absorption spectra of the PEGylated copper sulfide nanoparticles of 2.7 nm (black), 4.8 nm (red), and 7.2 nm (blue).

lated copper sulfide NPs form no aggregates in water.[37] Long-term (*ca.* 10 days) observations further demonstrate that the resulting particles possess excellent colloidal stability in water as well as PBS buffer that is commonly used for mimicking the biological conditions. All these data support the fact that HS-PEG can effectively render copper sulfide NPs satisfying water solubility and colloidal stability by suppressing the dipole–dipole interactions among copper sulfide NPs, probably due to the steric hindrance effect of HS-PEG. To verify this hypothesis, thioglycolic acid (TGA) was used instead of HS-PEG in the synthesis of copper sulfide NPs. The following DLS studies revealed that the TGA-capped NPs gradually formed large agglomerates within days (Fig. S2†).

Cytotoxicity of the PEGylated copper sulfide NPs

The cytotoxicity of the PEGylated copper sulfide NPs was evaluated through the MTT assays on the proliferation of HeLa cells. As is shown in Fig. 4, all the PEGylated copper sulfide NPs present nearly no toxicity to HeLa cells at concentration below 3 mg L^{-1}. The cell viability starts to decrease when the particle concentration is higher than 5 mg L^{-1}, but remains above 40% even when the particle concentration reaches 25 mg L^{-1}. The positive correlation of the cell viability with the particle size may be caused by the enhanced ion leakage of smaller NPs.[38–40] However, according to the literature reports,[18,21] if a dose of the copper sulfide NPs around 3 mg kg^{-1} is suitable for PA imaging, the current copper sulfide NPs are nearly nontoxic. Further theoretical fittings revealed that the IC_{50} (50% inhibitory concentration) values of CS-2.7, CS-4.8, and CS-7.2 are 5.7 μmol L^{-1}, 1.5 μmol L^{-1}, and 0.6 μmol L^{-1}, respectively, if the IC_{50} values are expressed against particle concentration rather than copper concentration (Fig. S3†).

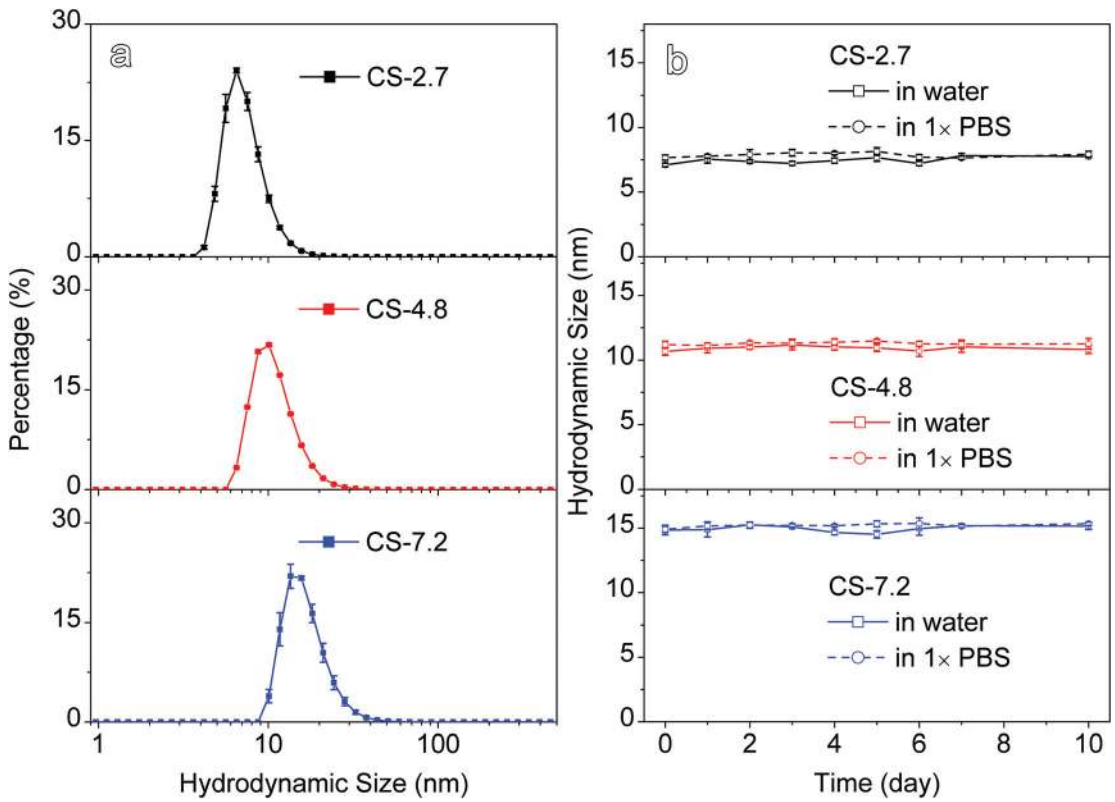

Fig. 3 The hydrodynamic size profiles of as-prepared 2.7 nm (black), 4.8 nm (red), and 7.2 nm (blue) copper sulfide nanoparticles, respectively (a), and temporal evolutions of the hydrodynamic sizes of the corresponding samples in water (square) and 1× PBS (circle), respectively (b).

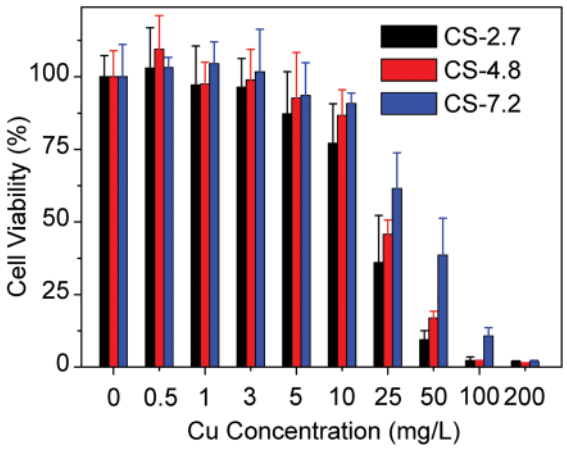

Fig. 4 Viability of HeLa cells recorded after being incubated with differently sized PEGylated copper sulfide nanoparticles with different Cu concentrations.

In vitro PA imaging of the PEGylated copper sulfide NPs

The PA imaging performance of PEGylated copper sulfide NPs was evaluated on a multispectral optoacoustic tomography system at room temperature. The upper frame of Fig. 5 shows three sets of PA images of aqueous solutions containing NPs of CS-2.7, CS-4.8, and CS-7.2. It can be seen that all the three NPs are presenting a dramatic PA effect. The quantified PA signals against Cu concentration reveal that the contrast enhancement effect is positively correlated to the particle size due to the size-dependent absorbance of copper sulfide NPs.[3,5,41]

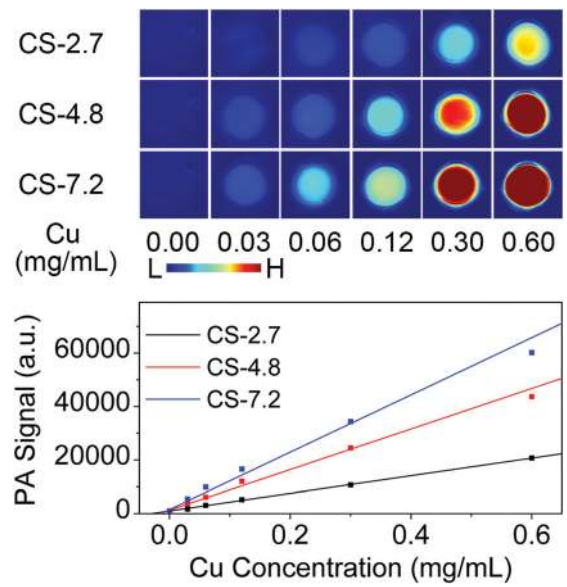

Fig. 5 *In vitro* photoacoustic imaging (upper frame) and the correspondingly quantified PA signal (lower frame) of aqueous solutions containing differently sized PEGylated copper sulfide nanoparticles.

In vivo PA imaging of tumors with the PEGylated copper sulfide NPs

To further show the PA contrast enhancement effect of the as-prepared copper sulfide NPs in tumor imaging, a subcutaneously transplanted tumor model bearing HeLa xenografts was adopted. 10 days after the inoculation of tumor cells, three groups of BALB/c nude mice (n = 4 per group) with comparable tumor sizes of 5–7 mm were selected to evaluate the PA imaging performance of copper sulfide NPs that were intravenously injected through the tail vein. A set of PA images of the tumor region acquired before and at different time points post-injection are presented in Fig. 6a. The overall contrast of the tumor sites was gradually enhanced and the enhancement effects at the tumor boundary (indicated by red arrows) became more significant, which is greatly meaningful for imaging guided surgery. Such a boundary enhancement effect was previously explained by the unique feature of absorption contrast in PA imaging.[42,43]

To further quantitatively evaluate the performance of the copper sulfide NPs, the PA signals of the region of interest (ROI) in each set of images are normalized and presented in Fig. 6b. The quantified results reveal that smaller particles produce dramatically increased contrasts for the tumor site than larger particles in the first 4 h of post-injection. Thereafter, the PA signals of tumors enhanced by both CS-2.7 and CS-4.8 NPs keep increasing and reach maximum values at around 24 h, while the PA signals of tumors enhanced by CS-7.2 NPs stop increasing after 8 h of post-injection. According to the results shown in the lower frame of Fig. 5, the PA signal generated with CS-7.2 NPs is approximately 62 times that with CS-2.7 NPs if normalizing the concentration by the molar concentration of NPs rather than Cu ions, *i.e.*, larger copper sulfide NPs produce stronger PA contrast than smaller copper sulfide NPs *in vitro*. While the quantified results shown in Fig. 6b reveal that the maximum contrast produced by CS-2.7 NPs (24 h) is 1.76 times that achieved by CS-7.2 NPs (8 h) although the dose of CS-2.7 is only 18 times higher than that of CS-7.2 NPs according to the molar concentration of nanoparticles. These quantified results suggest that the overall contrast enhancement of smaller particles is more significant than that of the larger ones for *in vivo* tumor imaging, which may be attributed to more effective tumor uptake of smaller NPs than the bigger ones. To confirm this hypothesis, further pharmacokinetic studies of differently sized PEGylated copper sulfide NPs were carried out on the Sprague Dawley rats and the results shown in Fig. 6c demonstrate that the blood half-time of the copper sulfide NPs is inversely proportional to the particle size, *e.g.*, 33 min for CS-2.7, 25 min for CS-4.8, and 20 min for CS-7.2. Since a long blood half-time is in favour of the extravasation of copper sulfide NPs from blood to the tumor through enhanced permeability of tumor blood vessels, the smaller particles presented a better PA contrast enhancement effect *in vivo*.[44,45]

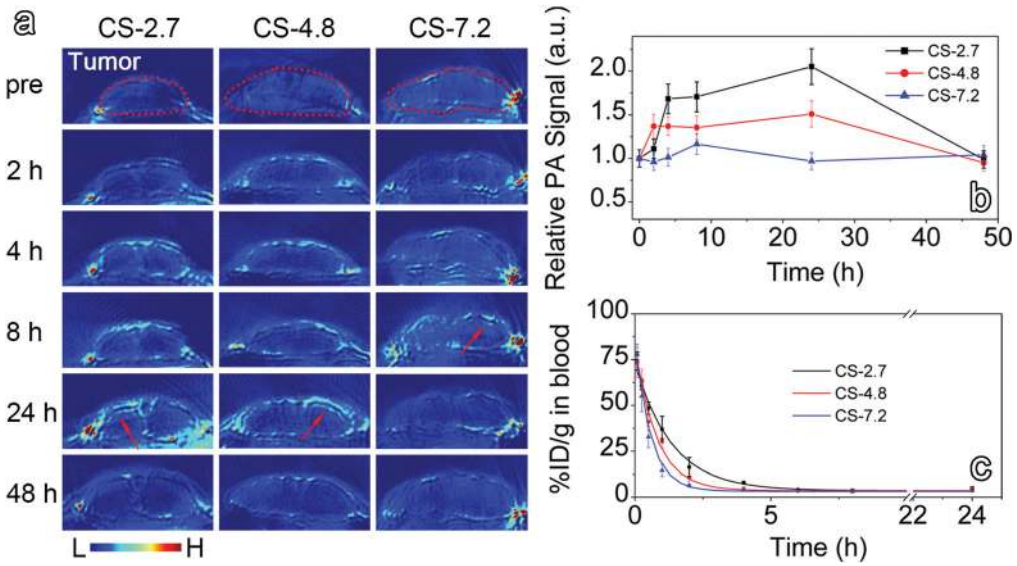

Fig. 6 *In vivo* photoacoustic images acquired pre- and at different time points after intravenous injection of the differently sized copper sulfide nanoparticles into the mouse bearing subcutaneous tumors (a), temporal evolution of the integrated photoacoustic signals recorded from the tumor region (b), and blood clearance profiles of differently sized copper sulfide nanoparticles in rats (n = 4) (c). The solid lines in frame (c) are theoretical fitting curves obtained through a single-compartment model for depicting the clearance behaviors of the nanoparticles.

Conclusions

In summary, we have successfully synthesized monodispersed PEGylated copper sulfide NPs through an aqueous synthetic route. The surface PEGylation rendered copper sulfide NPs excellent colloidal stabilities in both water and PBS buffer apart from a significant LSPR effect. The low cytotoxicity of the copper sulfide NPs enabled them to be potentially useful as a contrast agent for PA imaging. Although larger particles exhibit a stronger contrast enhancement effect, the following tumor imaging studies suggest that the small particles can more effectively enhance the contrast of the tumor boundary due to a prolonged blood half-time, which highlights the importance of strict particle size control for sensitive tumor imaging. It is worthy to mention that the tumor boundary can be more significantly enhanced by copper sulfide particles smaller than 5 nm, which is clinically meaningful for developing PA contrast agents for imaging guided tumor therapy.

Acknowledgements

The authors acknowledge funding from the National Basic Research Program of China (2011CB935800), the National Natural Science Foundation of China (21203210, 21321063, and 81090271), and ICCAS (CMS-PY-201309).

References

1 L. M. Nie and X. Y. Chen, *Chem. Soc. Rev.*, 2014, **43**, 7132–7170.
2 X. Yang, S. E. Skrabalak, Z.-Y. Li, Y. Xia and L. V. Wang, *Nano Lett.*, 2007, **7**, 3798–3802.
3 L. V. Wang and S. Hu, *Science*, 2012, **335**, 1458–1462.
4 T. Harrison, J. C. Ranasinghesagara, H. Lu, K. Mathewson, A. Walsh and R. J. Zemp, *Opt. Express*, 2009, **17**, 22041–22046.
5 W. Li and X. Chen, *Nanomedicine*, 2015, **10**, 299–320.
6 L. H. V. Wang, *Nat. Photonics*, 2009, **3**, 503–509.
7 L. H. V. Wang, *Dis. Markers*, 2003, **19**, 123–138.
8 R. Schulze, G. Zangerl, M. Holotta, D. Meyer, F. Handle, R. Nuster, G. Paltauf and O. Scherzer, *J. Biomed. Opt.*, 2011, **16**, 086002.
9 J. A. Viator, J. Komadina, L. O. Svaasand, G. Aguilar, B. Choi and J. S. Nelson, *J. Invest. Dermatol.*, 2004, **122**, 1432–1439.
10 Y. Wang, S. Hu, K. Maslov, Y. Zhang, Y. Xia and L. V. Wang, *Opt. Lett.*, 2011, **36**, 1029–1031.
11 J. V. Jokerst, A. J. Cole, D. Van de Sompel and S. S. Gambhir, *ACS Nano*, 2012, **6**, 10366–10377.
12 C. Kim, E. C. Cho, J. Chen, K. H. Song, L. Au, C. Favazza, Q. Zhang, C. M. Cobley, F. Gao, Y. Xia and L. V. Wang, *ACS Nano*, 2010, **4**, 4559–4564.
13 L. Nie, S. Wang, X. Wang, P. Rong, A. Bhirde, Y. Ma, G. Liu, P. Huang, G. Lu and X. Chen, *Small*, 2014, **10**, 1585–1593.
14 J. M. Luther, P. K. Jain, T. Ewers and A. P. Alivisatos, *Nat. Mater.*, 2011, **10**, 361–366.
15 X. Liu, X. Wang, B. Zhou, W.-C. Law, A. N. Cartwright and M. T. Swihart, *Adv. Funct. Mater.*, 2013, **23**, 1256–1264.
16 X. Liu and M. T. Swihart, *Chem. Soc. Rev.*, 2014, **43**, 3908–3920.
17 Y. Zhao, H. Pan, Y. Lou, X. Qiu, J. Zhu and C. Burda, *J. Am. Chem. Soc.*, 2009, **131**, 4253–4261.

18 G. Ku, M. Zhou, S. L. Song, Q. Huang, J. Hazle and C. Li, *ACS Nano*, 2012, **6**, 7489–7496.
19 S. Goel, F. Chen and W. B. Cai, *Small*, 2014, **10**, 631–645.
20 M. Zhou, G. Ku, L. Pageon and C. Li, *Nanoscale*, 2014, **6**, 15228–15235.
21 K. Yang, L. Zhu, L. M. Nie, X. L. Sun, L. Cheng, C. X. Wu, G. Niu, X. Y. Chen and Z. Liu, *Theranostics*, 2014, **4**, 134–141.
22 Y. Wu, C. Wadia, W. Ma, B. Sadtler and A. P. Alivisatos, *Nano Lett.*, 2008, **8**, 2551–2555.
23 Q. Y. Lu, F. Gao and D. Y. Zhao, *Nano Lett.*, 2002, **2**, 725–728.
24 C.-H. Kuo, Y.-T. Chu, Y.-F. Song and M. H. Huang, *Adv. Funct. Mater.*, 2011, **21**, 792–797.
25 Z. Zhuang, Q. Peng, B. Zhang and Y. Li, *J. Am. Chem. Soc.*, 2008, **130**, 10482–10483.
26 C. G. Tian, Z. H. Kang, E. B. Wang, L. Gao, C. L. Wang, L. Xu and C. W. Hu, *Mater. Lett.*, 2005, **59**, 1156–1160.
27 G. X. Ma, Y. L. Zhou, X. Y. Li, K. Sun, S. Q. Liu, J. Q. Hu and N. A. Kotov, *ACS Nano*, 2013, **7**, 9010–9018.
28 H. L. Cao, X. F. Qian, C. Wang, X. D. Ma, J. Yin and Z. K. Zhu, *J. Am. Chem. Soc.*, 2005, **127**, 16024–16025.
29 L. D. Partain, P. S. McLeod, J. A. Duisman, T. M. Peterson, D. E. Sawyer and C. S. Dean, *J. Appl. Phys.*, 1983, **54**, 6708–6720.
30 S.-C. Liufu, L.-D. Chen, Q. Yao and F.-Q. Huang, *J. Phys. Chem. C*, 2008, **112**, 12085–12088.
31 L. X. Yi and M. Y. Gao, *Cryst. Growth Des.*, 2011, **11**, 1109–1116.
32 W. Han, L. X. Yi, N. Zhao, A. W. Tang, M. Y. Gao and Z. Y. Tang, *J. Am. Chem. Soc.*, 2008, **130**, 13152–13161.
33 K. Ding, L. H. Jing, C. Y. Liu, Y. Hou and M. Y. Gao, *Biomaterials*, 2014, **35**, 1608–1617.
34 K. De Nolf, R. K. Capek, S. Abe, M. Sluydts, Y. Jang, J. C. Martins, S. Cottenier, E. Lifshitz and Z. Hens, *J. Am. Chem. Soc.*, 2015, **137**, 2495–2505.
35 Z. A. Peng and X. G. Peng, *J. Am. Chem. Soc.*, 2001, **123**, 1389–1395.
36 I. Grozdanov and M. Najdoski, *J. Solid State Chem.*, 1995, **114**, 469–475.
37 R. A. Sperling, T. Liedl, S. Duhr, S. Kudera, M. Zanella, C. A. J. Lin, W. H. Chang, D. Braun and W. J. Parak, *J. Phys. Chem. C*, 2007, **111**, 11552–11559.
38 Y. Pan, S. Neuss, A. Leifert, M. Fischler, F. Wen, U. Simon, G. Schmid, W. Brandau and W. Jahnen-Dechent, *Small*, 2007, **3**, 1941–1949.
39 M. V. D. Z. Park, A. M. Neigh, J. P. Vermeulen, L. J. J. de la Fonteyne, H. W. Verharen, J. J. Briedé, H. van Loveren and W. H. de Jong, *Biomaterials*, 2011, **32**, 9810–9817.
40 M. Baek, M. K. Kim, H. J. Cho, J. A. Lee, J. Yu, H. E. Chung and S. J. Choi, *J. Phys.: Conf. Ser.*, 2011, **304**, 012044.
41 X. D. Wang, Y. J. Pang, G. Ku, X. Y. Xie, G. Stoica and L. H. V. Wang, *Nat. Biotechnol.*, 2003, **21**, 803–806.
42 Z. Guo, L. Li and L. V. Wang, *Med. Phys.*, 2009, **36**, 4084–4088.
43 L. Nie, M. Chen, X. Sun, P. Rong, N. Zheng and X. Chen, *Nanoscale*, 2014, **6**, 1271–1276.
44 H. Maeda, H. Nakamura and J. Fang, *Adv. Drug Delivery Rev.*, 2013, **65**, 71–79.
45 N. Bertrand, J. Wu, X. Xu, N. Kamaly and O. C. Farokhzad, *Adv. Drug Delivery Rev.*, 2014, **66**, 2–25.